One-dimensional versus two-dimensional surface states on stepped Au(111)

J. E. Ortega,[1,2] A. Mugarza,[1,2] V. Repain,[3] S. Rousset,[3] V. Pérez-Dieste,[4] and A. Mascaraque[4]
[1]*Donostia International Physics Center and Centro Mixto de Materiales CSIC/UPV, Paseo Manuel Lardizabal 4, 20018-San Sebastian, Spain*
[2]*Universidad del País Vasco, Departamento de Física Aplicada I, Plaza de Oñate 2, E-20018 San Sebastian, Spain*
[3]*Groupe de Physique des Solides, CNRS, Universités Paris 6 et 7, 2 Place Jussieu, 75251 Paris Cedex 5, France*
[4]*LURE Centre Universitaire Paris-Sud, Bât 209D Boîte Postal 34, 91898 Orsay Cedex, France*
(Received 19 November 2001; published 4 April 2002)

Surface states at vicinal Au(788) and Au(322) have been investigated with angle-resolved photoemission and synchrotron radiation. Both surfaces are characterized by highly regular one-dimensional step arrays with relatively wide (~3.9 Å) or narrow (~1.3 Å) terraces in Au(788) and Au(322), respectively. Depending on the terrace size we observe that surface electrons behave in a completely different way. In Au(788) terraces become one-dimensional, lateral quantum wells that confine surface electrons between adjacent steps. In Au(322) surface electrons propagate across the step array forming two-dimensional superlattice bands. By tuning photon energy and angle we probe fundamental properties of the electron wave functions in both cases.

DOI: 10.1103/PhysRevB.65.165413 PACS number(s): 79.60.−i, 73.20.−r, 73.21.−b

I. INTRODUCTION

Vicinal surfaces are natural templates for self-assembling ordered arrays of nanowires and nanodots with tailored electronic states and transport properties.[1,2] They can also be used as model systems for studying the electron wave functions and other basic properties of lateral nanostructures.[3,4] Vicinal noble metal (111) surfaces are particularly suitable because their known p_z-like surface state scatters strongly at step edges.[5–8] Here we study this surface state at Au(322) and Au(788) surfaces, which are vicinal to the (111) plane. Both are characterized by highly regular step arrays over micron-size areas, making them ideal for photoemission studies. Although the basic structural difference between Au(322) and Au(788) is the terrace width (i.e., the period of the step superlattice), they display completely different electronic structures. In Au(322) we have relatively narrow (1.3 Å) terraces and the surface state is a two-dimensional band, folded at the center of the step superlattice Brillouin zone. In Au(788) the terraces are wider (3.9 Å) and the surface state breaks up into one-dimensional lateral quantum-well states. Such different behavior can be explained in the light of the different bulk band structure projection on each surface plane.

The photoemission experiments have been performed at the SU8 undulator, Spanish-French beam line at LURE (Paris). The experiments were done at 300 K using *p*-polarized light. The experimental station is equipped with an angle-resolved photoemission setup that provides an angular resolution lower than 0.5°. The total energy resolution is 50 meV. Au(322) is vicinal with respect to Au(111) by a miscut angle of 11.4° towards [211] and presents {100}-like steps. Au(788) has a miscut angle of 3.5° towards [211] and {111}-like steps. *In situ* surface preparation is done by extensive sputtering-annealing cycles. Most of Au(111) vicinals undergo facetting,[9] but Au(322) and Au(788) are stable orientations. Figure 1 shows the respective scanning tunneling microscopy (STM) images. We observe micron-size surface areas with defect-free, regular arrays of straight, monatomic ($h=2.35$ Å) steps. In Au(322) terraces are 1×1, (111) planes, whereas Au(788) terraces display a characteristic reconstruction that is similar to the reconstruction of Au(111).[9,10] This is better observed in the closer view shown in the inset of Fig. 1(b) where the corrugation due to the terrace levels has been subtracted. Discommensuration lines run perpendicular to the step edges indicating the presence of alternative fcc- and hcp-packed domains along a single terrace. In the bottom panel we show the terrace width distribution measured over 30 images and more than 200 terraces. The resulting average terrace width values are $d=13\pm2$ Å for Au(322) and $d=39\pm5$ Å for Au(788). In both cases the sharp terrace width distribution is expected from the strong elastic interaction between adjacent steps as well as from the high kink energy of gold. In Au(788) it is also possible that the highly homogeneous step array is related to the terrace reconstruction, as observed on Si(111).[11]

II. 1D VERSUS 2D SURFACE STATES

The flat Au(111) surface electronic structure is characterized by the presence of a well-known, free-electron-like, two-dimensional surface state close to the Fermi energy E_F in the center of the surface Brillouin zone.[12] At stepped Au(322) and Au(788) the free-electron-like character of the surface state is maintained parallel to the steps (*y* direction in Fig. 1), where we observe a parabolic dispersion with an effective mass $m^*=0.27m_e$ similar to the effective mass in Au(111).[4] The band dispersion is only affected in the direction perpendicular to the step array (*x* direction). Figures 2(a) and 2(b), respectively, contain the photoemission spectra of Au(322) and Au(788) near the Fermi level showing the dispersion of the surface state peak in the *x* direction. The emission angle is measured with respect to the surface normal. The differences between both surfaces are remarkable. The surface state peak disperses in Au(322), but it splits into two non-dispersing features in Au(788). This means that the surface state is a two-dimensional (2D) state for Au(322) and a one-dimensional (1D) state for Au(788).[13]

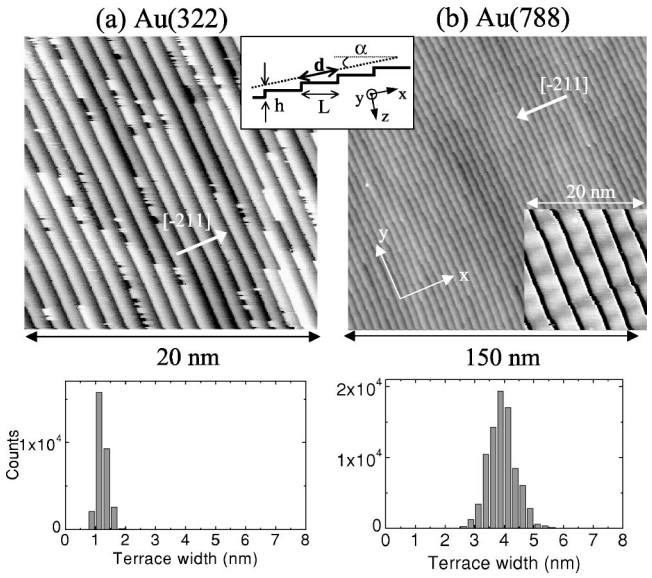

FIG. 1. STM pictures from (a) Au(322) and (b) Au(788) showing highly regular one-dimensional step arrays. The right inset shows the detailed structure of Au(788) terraces. Bright and dark areas indicate the presence of alternating fcc- and hcp-packed square areas within the same terrace (Ref. 9). The terrace width distribution for each surface is shown in the bottom panels. The top inset schematically depicts the side view of the one-dimensional step array, where miscut angle, step height, and terrace width appear defined.

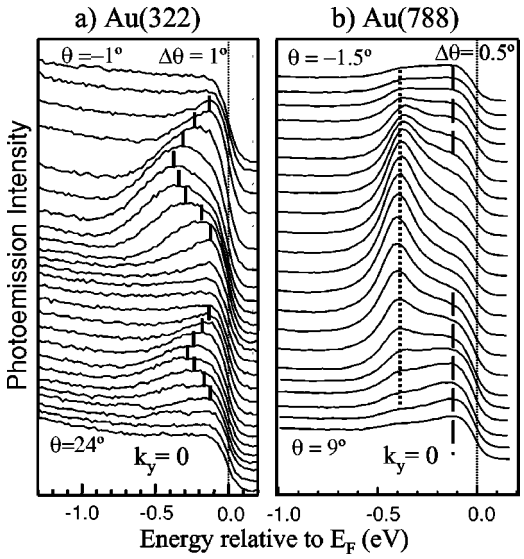

FIG. 2. Photoemission spectra showing the surface state dispersion in the direction perpendicular to the step array (x direction in Fig. 1) in (a) Au(322) and (b) Au(788). The emission angle θ is measured with respect to the surface normal and the photon energy is 27 eV. In Au(322), the surface state is a broad, 2D dispersing feature whereas in Au(788) it splits into two sharp, 1D nondispersing levels.

The $E(k_x)$ band dispersions in the direction perpendicular to the steps for both Au(322) and Au(788) are shown in Fig. 3. k_x is obtained from the emission angle θ and the (measured) kinetic energy via the known equation $k_x = \sqrt{(2m/\hbar^2)E_{kin}}\sin\theta$. All the energies are referred to the Fermi level E_F. For Au(322) data points in Fig. 3(a) are determined directly from the peak maxima in the spectra in Fig. 2(a) (tick marks). They are fitted with two parabolas. These appear symmetric with respect to the surface Brillouin zone center, suggesting band folding by step superlattice vectors. The band centers are located at $k_x = 0.23 \pm 0.04$ Å^{-1} and $k_x = 0.74 \pm 0.04$ Å^{-1}, consistent with $g/2 = \pi/d = 0.25$ Å^{-1} and $3g/2 = 3\pi/d = 0.74$ Å^{-1}, respectively. The shift of the p_z-like surface band to the surface Brillouin zone edge is expected for vicinal surfaces, as explained in Sec. V. The band minimum is found at $E_{min} = -0.36$ eV in the first Brillouin zone and slightly higher in the second zone. This appears to be an artifact related to the lower intensity of the folded band.[14] Within the error bars, the effective mass deduced from the parabolic fit is $m^* = 0.28 m_e$, which is again similar to the effective mass in Au(111), indicating that the scattering at the step edges is weak in Au(322). Assuming a one-dimensional Kronig-Penney model with δ-function-like step potentials, the strength of the step barrier can be estimated from the upwards shift of the superlattice band with respect to the flat surface band.[15] Although the correct reference is the energy of the infinite fcc-packed terrace we can use the surface state energy of Au(111), since its herringbone reconstruction only results in minor energy changes.[10] The surface state of Au(111) has been measured separately under the same experimental conditions, giving $E_F - E_0 = -0.46$ eV. Thus we obtain $\Delta E = E_{min} - E_0 = 0.1$ eV. Following the analysis of Ref. 15, we deduce a repulsive barrier of ~ 1.4 eV Å^{-1} and a transmission probability $|T| = 0.84$ at monatomic steps in Au(322). These values are similar to those found in Cu(111) vicinals.[15]

The data points in Fig. 3(b) for Au(788) are obtained from a line fitting to the spectra in Fig. 2(b), which gives the accurate energy position and the intensity of the two 1D features. The fitting uses asymmetric Lorentzian lines for the peaks, plus a Shirley and a polynomial background, all convoluted with a Gaussian to account for the overall energy resolution. We clearly observe two flat levels at -0.40 eV

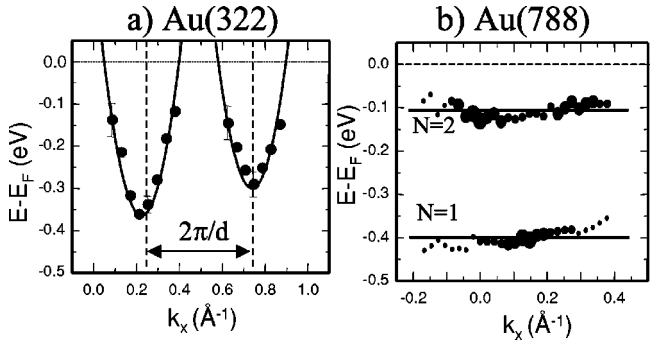

FIG. 3. $E(k_x)$ surface bands corresponding to the spectra of Fig. 2. In Au(322), the surface state forms superlattice bands (zone folded by $g = 2\pi/d$), whereas in Au(788) we observe two 1D quantum-well levels. The size of the dots in (b) is proportional to the corresponding peak intensity in Fig. 2(b). The energy gap between quantum levels in Au(788) is consistent with total electron confinement within terraces.

and -0.11 eV, suggesting strong confinement along the k_x direction. If we assume the terraces in Au(788) as infinite quantum wells of size L, the energy of the N th level, referred to the ground state of the infinitely wide terrace E_F-E_0, is given by

$$E_N=E_F-E_0+\frac{\hbar^2\pi^2}{2m^*L^2}N^2. \tag{1}$$

The energy gap between the two levels in Fig. 3(b) agrees with the energy interval between the lowest two levels of this infinite one-dimensional quantum well, i.e., $(2^2-1^2)\times[(\hbar^2\pi^2)/(2m^*L^2)]=0.28$ eV, where $m^*=0.27m_e$ and $L=39$ Å. We conclude that surface electrons are strongly confined within individual terraces at the Au(788) step array, in the same way as they get confined within isolated terraces in Au(111) and Ag(111).[5,6]

Using Eq. (1) and the absolute energy of the quantum levels in Fig. 3(b) we obtain $E_F-E_0=-0.50$ eV. This value is different from $E_F-E_0=-0.46$ eV measured in Au(111). Assuming the latter as the reference energy of the infinitely wide terrace, such deviation could indicate that the actual terrace potential in Au(788) is not the ideal infinite quantum well. In this sense note that the data points in Fig. 3(b) display some random variation within the error bars that can be interpreted as a narrow band. Using the Kronig-Penney model, the width of the band allows to estimate an upper limit for the transmission probability across the step barrier. We obtain a maximum value of $|T|=0.1$ and $|T|=0.19$ for the first and the second levels, which are still considerably smaller than those found for Au(322). For this value of T and within the same Kronig-Penney model we obtain $E_F-E_0=-0.48$ eV, i.e. closer to the energy of the Au(111) surface state.[16]

III. MAPPING THE WAVE FUNCTION AT LATERAL QUANTUM WELLS

The size of the data points in Fig. 3(b) reflects the normalized photoemission intensity (area under the peak) of the 1D quantum-well levels in Au(788). Such intensity is shown in Fig. 4(a) as a function of the emission angle. It thus represents the experimental angle-resolved photoemission matrix element in the direction perpendicular to the steps for the two terrace quantum levels. We can estimate such matrix element using Fermi's golden rule for optical transitions,

$$I\propto|\langle\psi_i|\mathbf{A}\cdot\mathbf{p}|\psi_f\rangle|^2 \tag{2}$$

Here $\mathbf{A}$ and $\mathbf{p}$, respectively, correspond to the light vector potential and the momentum operators, and ψ_i and ψ_f to the electron wave functions in the initial (quantum-well) and the final states, respectively. At a terrace we can approach the initial state wave function as the product of a wave decaying into the bulk, a plane wave parallel to the terrace, and the wave function in the x' direction, i.e., $\psi_i(x',y',z')=e^{-\kappa z'}e^{ik_{y'}\cdot y'}\psi_{k_{x'}}(x')$. The (x',y',z') reference system is defined in the (111) terrace plane, as depicted in the inset of Fig. 4(a). The matrix element can be simplified assuming the final-state wave function as a plane wave $\psi_f=e^{i\mathbf{q}\cdot\mathbf{r}}$. With p polarization $\mathbf{A}\simeq A_z\hat{\mathbf{k}}$ and making $q_{y'}=0$, Eq. (2) is reduced to

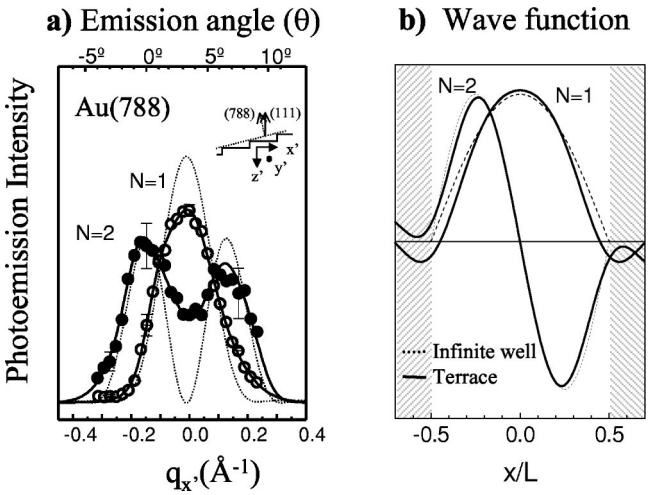

FIG. 4. (a) Photoemission intensity for the two quantum-well levels of Fig. 1(b). Such intensity reflects the probability density of the one-dimensional terrace quantum-well states in Au(788). It fits to the probability density for the corresponding quantum-well states of the 1D infinite potential well (dashed lines) calculated in the $x'y'z'$ reference system of the terraces (inset), indicating that both share similar wave functions. (b) Wave functions in real space for the terrace quantum well obtained from (a), compared with the infinite quantum-well wave functions.

$$I(q_{x'})\propto|\langle e^{-\kappa z'}|A_zp_z|e^{q_{z'}z'}\rangle|^2|\langle\psi_{k_{x'}}(x')|e^{q_{x'}x'}\rangle|^2. \tag{3}$$

At the photon energy used in the experiment and close to the surface normal $q_{z'}$ ($q_{z'}\gg q_{x'},q_{y'}$) is fixed by energy conservation. The first term in Eq. (3) is thus constant, and the matrix element is only a function of the second term, which is written as

$$I(q_{x'})\propto\left|\int e^{iq_{x'}\cdot x'}\psi_{k_{x'}}(x')dx'\right|^2. \tag{4}$$

where $q_{x'}$ is the final-state wave vector along the x' direction that is fixed by the emission angle. Equation (4) is describing the 1D wave function probability density $|\psi(q_{x'})|^2$ in reciprocal space, which is the analog of the charge density mapped in real space by STM.[5,6] By chosing a plane wave for the final state we neglect the effect of the step superlattice, which results in a smooth modulation of Eq. (4). In our analysis we avoid this modulation by chosing a photon energy such that the interference effect of the superlattice is canceled.[17] Within the limits of the approach made to the matrix element, we can conclude that the probability density in reciprocal space for $N=1$ and $N=2$ in the terrace quantum well is being obtained experimentally in Fig. 4(a). It is thus interesting to compare this result with the infinite, one-

dimensional quantum well of size L. In this case we have the well-known wave functions $\psi_N(x')=\sin(\pi N x'/L)$ that allow us to simplify Eq. (4) to give

$$I_{QW_\infty}(q_{x'})=A\frac{1-(-1)^N\cos(q_{x'}L)}{\left[q_{x'}^2-\left(\frac{\pi N}{L}\right)^2\right]^2}N^2, \tag{5}$$

where A is a normalization constant that can be chosen to make the total intensity $\int I_{QW_\infty}(q_{x'})dx'$ equal to the area under the experimental intensity curve for $N=1$. With this value of A we obtain the dotted lines shown in Fig. 4(a) for $N=1$ and $N=2$ of the infinite quantum well. Peak positions are well reproduced, indicating that the terraces effectively behave as infinite potential wells with similar wave functions. Actually, from Eq. (4) we deduce that the wave function in real space can be obtained experimentally from $I(q_{x'})$ by Fourier transformation. The missing phase is determined by supposing a symmetric well, and therefore only even or odd wave functions. Using the data in Fig. 4(a) we obtained the wave functions in real space for the terrace quantum well. The result is shown in Fig. 4(b), together with the wave functions of the infinite quantum well. We observe small differences that can be due to the actual shape of the terrace potential. However, the differences lie within the error bars of the experiment and the approach used to simplify the matrix element in Eq. (2). A more refined, quantitative analysis requires a better theoretical approach of this matrix element, especially in order to account for photoemission final-state effects. This analysis is in progress.[17]

IV. THREE-DIMENSIONAL FOURIER ANALYSIS BY PHOTON ENERGY TUNING

The center of the probability density functions in Fig. 4(a) is shifted by 3.5° from the surface normal. This angle corresponds to the direction perpendicular to the (111) plane, proving that this plane is the appropriate reference of the 1D terrace potential in Au(788). In contrast the 2D surface state in Au(322) is modulated on the (322) average plane of the surface. This can be shown by probing the Fourier components of the surface wave function in the perpendicular direction, which in turn can only be done by tuning the photon energy in photoemission.[3] The analysis is presented in Figs. 5 and 6. In Fig. 5 we show the spectra from Au(322) along the x direction for increasing photon energies. The photoemission intensity is now shown in a gray scale, such that surface bands are directly observed. The most remarkable feature is the intensity shift from the first to the second superlattice Brillouin zone as the photon energy increases. The situation resembles that of the electron diffraction from a stepped surface, where the split spots are only observed under out-of-phase interference conditions.[18] In the present case the relative intensity of the zone-folded bands is explained by the spectral composition of the surface state perpendicular to the surface (z direction). This is demonstrated in the wave vector plot shown in Fig. 6. To simplify the discussion, we limit ourselves to the lowest electron energy, i.e. the surface band minima in Fig. 5. At the band minima

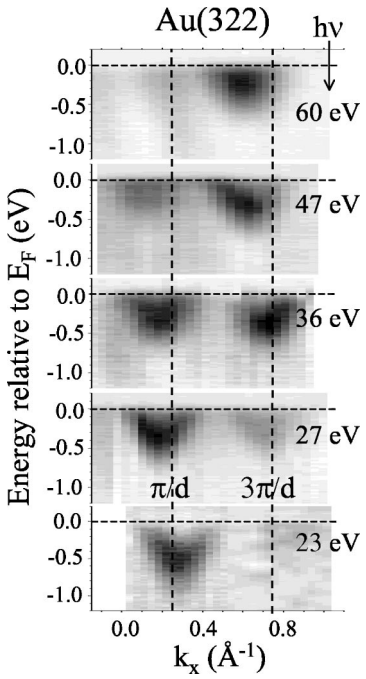

FIG. 5. Photoemission spectra of Au(322) measured at different photon energies are shown in a gray scale. The 2D, zone-folded surface bands along k_x are directly obtained. The photon energy dependent intensity of each band is related to the spectral weight of the different surface state Fourier components, which are selectively probed at every energy (see Fig. 6).

we measure the photoemission intensity normalized to the photon flux (size of the dots) and calculate the wave vector component perpendicular to the surface for the excited photoelectron out of the crystal (k_z^{out}). The latter is obtained from the electron kinetic energy E_{kin} and k_x by assuming constant energy lines ($k_y=0$)

$$E_{kin}=\frac{\hbar^2}{2m}[k_x^2+(k_z^{out})^2]. \tag{6}$$

Therefore, data points in Fig. 6(a) correspond to the photoemission final state outside the crystal. In the initial state (surface state) the wave vector components parallel to the surface k_x and k_y are the same as in the final state, since both are conserved in the photoemission process. k_z is not strictly conserved but broadened due to the lack of symmetry of the crystal in the z direction. In order to find the approximate value of k_z it is necessary to use bulk band calculations to find, first, the corresponding final state inside the crystal at the same energy, and then assume wave vector conservation in the reduced Brillouin zone. In Fig. 6 we have located the high-symmetry L point of the bulk Brillouin zone for the initial state, which is probed at ~26 eV and ~50 eV above E_F.[19] The photoemission intensity (size of the data points) is maximum close to this L point and decreases slowly away from it in the perpendicular direction. This k_z-dependent intensity is similar to that found in flat crystals and reflects the spectral composition of the wave function in the surface state along the direction perpendicular to the surface.[20] Such k_z

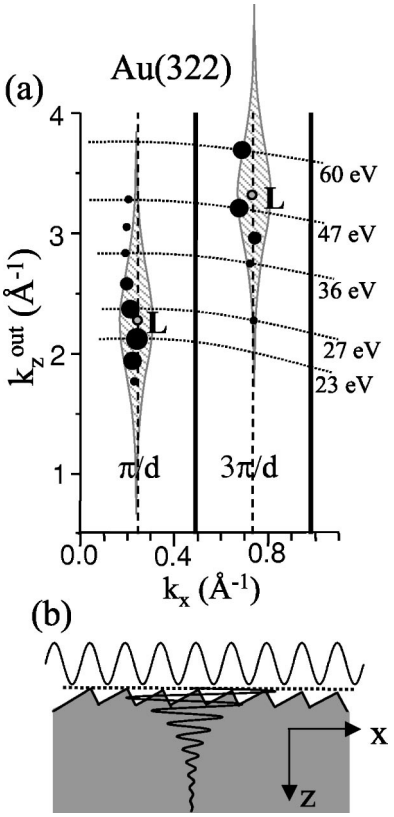

FIG. 6. (a) k_z^{out} and k_x wave vector components of photoelectrons out of the crystal. The data correspond to the band minima in Fig. 5. The size of the dots is proportional to the peak intensity. This is maximum near the L point of the bulk band structure which is probed at two different energies in the first and the second Brillouin zones. The plot reflects the spectral composition of the surface state wave function, as qualitatively described by the dashed cone. The corresponding wave function is described in real space in (b). Along the x direction, we have Bloch waves of the step superlattice. Along the z direction, the superlattice wave function is an evanescent wave with $k_z = k_L$, consistent with the k_z broadening shown in (a).

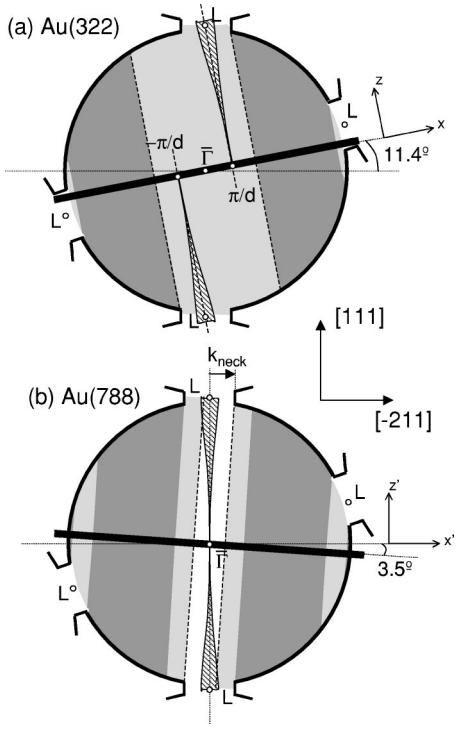

FIG. 7. Schematic projection of bulk states at E_F on (a) Au(322) and (b) Au(788). The dashed cones represent the Fourier spectrum of 2D and 1D surface states, which are projected differently at π/L in Au(322) and around $\bar{\Gamma}$ in Au(788). π/d 2D states in Au(322) mix with projected bulk states, whereas $\bar{\Gamma}$ 1D states are truly gap states. Such a different mixing explains their different dimensionality (see the text).

broadening around L, which is actually the consequence of the two-dimensional confinement in the surface plane, is depicted schematically in Fig. 6(a) with the dashed cones. Thus Fig. 6(a) provides a (qualitative) three-dimensional description of the superlattice wave function in the reciprocal space where all the Fourier components $(k_x, k_y = 0, k_z)$ are being probed and weighted.[21] The corresponding wave function in the real space is depicted in Fig. 6(b). Along the x direction, it is composed of Bloch waves with the periodicity of the superlattice. Along the z direction, it is an evanescent oscillation with $k_z = k_L$, consistent with the k_z broadening away from the L point.

V. BULK BAND STRUCTURE PROJECTION ON THE VICINAL PLANE

In order to understand the different nature of the surface state in Au(788) and Au(322) we examine the bulk band structure projection on each surface plane and along the direction perpendicular to the steps. This is shown schematically in Fig. 7. The vicinal surface plane is represented by a thick solid line rotated by the corresponding miscut angle about the (111) plane. The circles describe the bulk Fermi surface in the first Brillouin zone with its characteristic necks of width $k_{neck} = 0.24$ Å^{-1}.[12] Dark shaded regions indicate the projection of bulk states from the two halves of the Fermi surface, whereas light shaded areas correspond to bulk states projected from one side of the Fermi surface. Only in the case of Au(788) the projection of the two necks overlaps, leading to a gap around $\bar{\Gamma}$. The dashed cones in Fig. 7(a) represent the same Fourier spectrum of the 2D surface state in Au(322) probed in Fig. 6(a), which is characterized by the k_z broadening along the surface normal. In Fig. 7(b) the dashed cones indicate that 1D terrace quantum-well states in Au(788) have $k_{z'}$ broadening along the (111) terrace normal. This is concluded from the probability density functions shown in Fig. 4(a), which are centered around the (111) direction. Note that all the Fourier components of the 2D surface state in Au(322) lie at the L-point projection on the surface, i.e., at π/d. In contrast, the Fourier components of the 1D surface states of Au(788) with $k_{z'}$ broadening along the (111) direction lie at the $\bar{\Gamma}$ gap. This means that these 1D terrace quantum-well states are truly gap states, whereas 2D surface states of Au(322) are resonances that overlap with projected bulk states.

The different degree of coupling between projected bulk states and $\bar{\Gamma}$ and π/d surface states explains their different dimensionality. Gap states are sharply confined to the surface plane and they feel a strong step barrier potential. Mixing of π/d states with bulk states displaces the center of gravity of the electron wave function deeper in the bulk, and hence π/d states sense a smoother effective potential at the step.[22] For a low effective barrier the electron tunneling across the step can lead to significant terrace to terrace coupling, and hence to 2D superlattice band formation. The stronger surface-bulk mixing of π/d surface resonances is also supported by the recent line shape analysis done by Baumberger *et al.* in Cu(111) vicinals.[8]

Figure 7 suggests a transition from $\bar{\Gamma}$ states to π/d states as a function of the miscut angle. Such transition has been indeed observed in Cu(111) vicinals with about 7° miscut, i.e., when the $\bar{\Gamma}$ gap gets closed at the energy range of the surface state.[3,23] As deduced from Fig. 7(b), the gap at E_F closes in Au(111) vicinals with $\alpha_c = \arctan(k_{neck}/k_L) = 10.2°$ miscut. Thus for larger angles, as in Au(322), surface states at $\bar{\Gamma}$ are not longer supported. However, the data for Cu(111) vicinals indicate that significant tunneling across the step barrier occurs before the spectral weight is transferred from $\bar{\Gamma}$ to π/d. Indeed in Cu(111) with 5° miscut the surface state displays $\bar{\Gamma}$-like character [k_z' broadening along (111) terraces], though it is already a 2D dispersing band.[3] This appears to be again a consequence of the surface-bulk mixing that occurs during the $\bar{\Gamma}$ gap closing. For 5° the $\bar{\Gamma}$ gap in Fig. 7(b) has shrunk, such that part of the $\bar{\Gamma}$ state Fourier components overlap with bulk states.[23] As a result, the $\bar{\Gamma}$ state senses a lower effective step barrier and eventually becomes a 2D surface state.

VI. CONCLUSIONS

In summary, we observe that the p_z-like surface state can have one-dimensional or two-dimensional character at vicinal Au(111) surfaces depending on the terrace size. It is completely confined within wide terraces in Au(788) and becomes a two-dimensional, step superlattice state at narrow terraces in Au(322). Both surfaces represent the two limiting cases of a lateral nanostructure. This can be generally defined as a regular array of nano-sized objects on a surface. In Au(788) we have the case of individual, non interacting objects (terraces) that display quantum-well levels. In Au(322) effective barriers are lower and the object-to-object interaction is switched on, thereby leading to 2D superlattice bands. By means of angle-resolved photoemission and synchrotron radiation we can obtain, in both cases, the Fourier spectrum of the relevant electronic states, which is in turn necessary to properly describe the wave functions of the lateral nanostructure.

ACKNOWLEDGMENTS

A.Mu. and J.E.O. are supported by the Universidad del País Vasco (1/UPV/EHU/00057.240-EA-8078/2000). V.R. and S.R. are supported by the CNRS-ULTIMATECH program, the CRIF and the Université de Paris 7. V. P.-D. is supported by the Comunidad Autónoma de Madrid (Project No. 07N/0042/98) and the DGICYT (Spain) (Grant No. PB-97-1199). The experiments performed at LURE were funded by the Large Scale Facilities program of the European Union. Critical reading of the manuscript by F. J. Himpsel and F. J. García de Abajo is acknowledged. Technical support from the Spanish-French beam line staff is gratefully acknowledged.

[1] F.J. Himpsel, J.E. Ortega, G.J. Mankey, and R.F. Willis, Adv. Phys. **47**, 511 (1998).

[2] R. Nötzel and K.H. Ploog, Adv. Mater. **5**, 22 (1993); R. Nötzel, Z. Niu, M. Ramsteimer, H.P. Schönherr, A. Trampert, L. Däweritz, and K.H. Ploog, Nature (London) **392**, 56 (1998); P. Segovia, D. Purdie, M. Hegsberger, and Y. Baer, *ibid.* **402**, 504 (1999).

[3] J.E. Ortega, S. Speller, A.R. Bachmann, A. Mascaraque, E.G. Michel, A. Närmann, A. Mugarza, A. Rubio, and F.J. Himpsel, Phys. Rev. Lett. **84**, 6110 (2000).

[4] A. Mugarza, A. Mascaraque, V. Pérez-Dieste, V. Repain, S. Rousset, F.J. García de Abajo, and J.E. Ortega, Phys. Rev. Lett. **87**, 107601 (2001).

[5] Ph. Avouris and I.-W. Lyo, Science **264**, 942 (1994).

[6] L. Bürgi, O. Jeandupeux, A. Hirstein, H. Brune, and K. Kern, Phys. Rev. Lett. **81**, 5370 (1998).

[7] X.Y. Wang, X.J. Shen, and R.M. Osgood, Jr., Phys. Rev. B **56**, 7665 (1997).

[8] F. Baumberger, T. Greber, and J. Osterwalder, Phys. Rev. B **64**, 195411 (2001).

[9] V. Repain, J.M. Berroir, B. Croset, S. Rousset, Y. Garreau, V.H. Etgens, and J. Lecoeur, Phys. Rev. Lett. **84**, 5367 (2000).

[10] W. Chen, V. Madhavan, T. Jamneala, and M.F. Crommie, Phys. Rev. Lett. **80**, 1469 (1998).

[11] J. Viernow, J.-L. Lin, D.Y. Petrovykh, F.M. Leibsle, F.K-. Men, and F.J. Himpsel, Appl. Phys. Lett. **72**, 948 (1998).

[12] F. Reinert, G. Nicolay, S. Schmidt, D. Ehm, and S. Hüfner, Phys. Rev. B **63**, 115415 (2001).

[13] These strong differences between Au(322) and Au(788) do not appear to be related to the different step type of each surface. Photoemission (STM) experiments on Cu (Ag) vicinals with {100}-like and {111}-like step types and similar miscut angles display analogous band dispersion (confinement) (Refs. 4, 6, and 8).

[14] Split bands are identical when the second peak becomes stronger at higher photon energies (see Fig. 5).

[15] O. Sánchez, J.M. García, P. Segovia, J. Alvarez, A.L. Vázquez de Parga, J.E. Ortega, M. Prietsch, and R. Miranda, Phys. Rev. B **52**, 7894 (1995).

[16] Photoemission experiments on Au(111) can give different values for $E_F - E_0$ depending on the measuring conditions. In the most recent high resolution experiments at 300 K it is found $E_F - E_0 = -0.42$ eV [S. LaShell, B.A. McDougall, and E. Jensen,

Phys. Rev. Lett. **77**, 3419 (1996)]. Considering as well that the infinitely wide terrace like that of Au(788) has a different reconstruction than Au(111), it appears to be a large uncertainty in the correct reference energy for Eq. (1).

[17] F. J. García de Abajo *et al.* (unpublished).

[18] M. Henzler, Appl. Phys. (Berlin) **9**, 11 (1976).

[19] The 50 eV transition corresponds to the primary cone, free-electron-like final-state band folding at *L*, whereas the 26 eV one must be related to a secondary cone, free-electron band, as shown in R. Matzdorf, Surf. Sci. Rep. **30**, 153 (1998).

[20] P. Thiry, D. Chandesris, J. Lecante, C. Guillot, R. Pinchaux, and Y. Petroff, Phys. Rev. Lett. **43**, 82 (1979).

[21] The quantitative Fourier map requires the line shape analysis of the *L*-point resonance in Fig. 6(a). In principle, the width of the resonance allows one to obtain directly the penetration depth of the surface state inside the bulk (Ref. 20), shown as an evanescent tail in Fig. 6(b). However, the resonance width is a convolution of the k_z broadening of the surface state and the energy broadening of the final state. Since the latter is a very flat band at 26 eV (Ref. 19), the (unknown) final-state broadening becomes the dominant contribution. In this context, the numerical estimation of the penetration depth of the surface state becomes very unreliable.

[22] A similar behavior is found in image states at Cu(111) vicinals, which display and increasing sensitivity to the step barrier potential as they get physically closer to the surface (Ref. 7).

[23] J.E. Ortega, A. Mugarza, A. Närmann, A. Rubio, S. Speller, A.R. Bachmann, J. Lobo, E.G. Michel, and F.J. Himpsel, Surf. Sci. **482-485**, 764 (2001).